ELSEVIER

Journal of Nuclear Materials 296 (2001) 256–264

journal of nuclear materials

www.elsevier.com/locate/jnucmat

Embrittlement of the martensitic steel 91 tested in liquid lead

G. Nicaise *, A. Legris, J.B. Vogt, J. Foct

Laboratoire de Métallurgie Physique et Génie des Matériaux UMR CNRS 8517, Université de Lille 1, Bât. C6–2éme Etage, 59655 Villeneuve d'ascq cedex, France

Abstract

Two potential problems are encountered in the case of intimate contact between liquid metals and metallic substrates: grain boundary wetting and liquid metal embrittlement (LME) which both induce a degradation of the mechanical properties. Tensile tests were carried out on a 9% Cr 1% Mo martensitic (Grade 91) steel in a liquid lead environment at temperatures ranging between 623 and 773 K. The Grade 91 steel was submitted to heat treatments in order to modify its hardness and also to produce either ferritic or martensitic grains. Smooth and notched specimens were used. We found out that by combining adapted heat treatments and the notch effect, it is possible to create conditions severe enough that lead to LME. Our experimental observations (transgranular failure) are compatible with the expectations of traditional mechanisms based on a reduction of the surface energy and/or adsorption induced chemical bond softening at the steel surface in contact with liquid lead.

1. Introduction

Liquid metal embrittlement (LME) refers to the instantaneous reduction or loss of ductility of an otherwise ductile material when stressed in contact with liquid metal. Since the first known report of this phenomenon by Johnson [1], several review articles have been published since 1960. We refer the reader for instance to those of Kamdar [2], Stoloff [3], Fernandes and Jones [4] and more recently Joseph et al. [5]. Although several different mechanisms are discussed in these reviews, it is possible to separate them in two main classes: the dissolution/diffusion-based models and the adsorption/reduction of cohesion ones.

Another aspect of LME usually mentioned is its specificity [6,7], which means that only some particular liquid metal–solid metal couples are prone to embrittlement. Such a specificity has been recently questioned by Fernandes and Jones [8] who suggest that it may rely on particular testing conditions rather than on the actual interactions between the liquid and the solid metal.

Let us recall that the 9% Cr 1% Mo martensitic steel frequently designated Grade 91 is a good candidate as structural material in a spallation target environment containing liquid lead because it exhibits good swelling and creep resistance under irradiation up to 773 K and it is subjected to a reduced dissolution in lead due the absence of Ni. This work concerns thus a conceptual problem that has an important technological impact.

Literature reports that the hardest materials are generally more severely embrittled [2,4,5]. This suggests to carry out detailed investigations on martensitic steels because the large variation in the hardness can result from appropriate heat treatments. Indeed LME of the Grade 91 steel by liquid lead has been demonstrated in a previous paper [9]. The objective of this paper is to analyse more deeply the effects of some key parameters such as the influence of the test temperature and of the microstructure (ferritic or martensitic) on the LME phenomenon.

2. Experimental procedure

2.1. Base material

The base material used is the Z10 CD Nb V 9-1 steel designated Grade 91 and was supplied by Creusot Loire

* Corresponding author. Tel.: +33-3 20 33 62 23; fax: +33-3 20 43 40 40.

E-mail address: gregory.nicaise@univ-lille1.fr (G. Nicaise).

0022-3115/01/$ - see front matter
PII: S0022-3115(01)00525-6

Table 1
Chemical composition of the steel G91 used in this work

Element	Cr	Mo	V	Mn	Si	Ni	C	Nb	Fe
Weight %	8.80	1.00	0.25	0.38	0.41	0.17	0.11	0.07	Bal.

Industries. Its chemical composition is displayed in Table 1. The as-received material has a tempered martensitic microstructure resulting from the heat treatment consisting of 1 h at 1323 K, air quenching, 1 h at 1023 K and then air cooling. This microstructure was evidenced by optical observations using Vilella's reagent and by transmission electron microscopy (TEM) observations.

2.2. Specimen preparation, tensile tests and hardness measurements

Cylindrical tensile specimens with a 4 mm diameter and a gauge length of 20 mm were machined from the as-received plates. The specimens were then separated in three sets and submitted to different heat treatments summarised in Table 2. All the heat treatments start by austenising at 1323 K. HT0 and HT1 differ by their tempering temperature after quenching. No quench was done for HT2 but the temperature was decreased from 1323 to 973 K during approximately 3 h and then was held at 973 K during 24 h. These treatments were inferred from the CCT diagram of Grade 91steel (Fig. 1) [18]. After the heat treatment, a cylindrical notch 500 μm in depth and 200 μm in curvature radius was mechanically machined on some specimens. In Table 2 is also presented the nomenclature for the different types of specimens that will be used in this work. The tensile tests were performed at an initial strain rate of 10^{-4} s^{-1} and constant stroke speed using a Schenck RMC 100 servo-electric test machine. A schematic view of the experimental set-up is presented in Fig. 2. The test temperature, in the range 623–773 K (the melting point of lead is 600 K), was reached using a standard three heating zone furnace. The temperature was regulated and measured by a thermocouple attached to the gauge length of the specimen.

Vicker's hardness measurements were performed on a Mitutoyo AVK-C1 hardness tester under a 300 N load. One hardness value corresponds to the average of ten experimental measurements.

Two types of environment were tested: the air environment and the liquid lead. During a tensile test in air environment, the reservoir surrounding the specimen was filled with sand in order to ensure a good temperature homogeneity and stability.

During all these tests, the environment (sand or lead) stayed in contact with the ambient atmosphere so that no particular care was taken to control or measure the oxygen activity that was given by its atmosphere equilibrium value at the temperature of interest. The mechanical tests were started when the test temperature was reached. This took approximately 2 h for the longest test performed at 773 K. The mechanical test duration (some minutes) was negligible compared to the heating time. In any case, the total time of contact between liquid lead and the specimens was at most about an hour, that is much smaller than the time usually spent by some authors to prewet the specimens. For comparison, Rabkin et al. [10] imposed contact times between tin and an Fe–5 at.% Si steel up to 50 h at 1065 K when they studied the grain boundary wetting transition temperature. Such high temperatures are out of the scope of this

Table 2
Specimen characteristics and nomenclature[a]

Specimen type	Heat treatment	Hardness (HV30)	Notch parameters
			ρ = curvature radius, d = depth
HT0	Base material	250	–
HT0-N	Base material	250	$\rho = 200\,\mu m$ $d = 500\,\mu m$
HT1	1323 K–1 h, air quench 773 K–1 h, air cool	400	–
HT1-N	1323 K–1 h, air quench 773 K–1 h, air cool	400	$\rho = 200\,\mu m$ $d = 500\,\mu m$
HT2-N	1323 K–1 h 1323–973 K–3 h 973 K–24 h, air cool	150	$\rho = 200\,\mu m$ $d = 500\,\mu m$

[a] The figure after the name refers to the heat treatment and the letter N means 'notched specimen'.

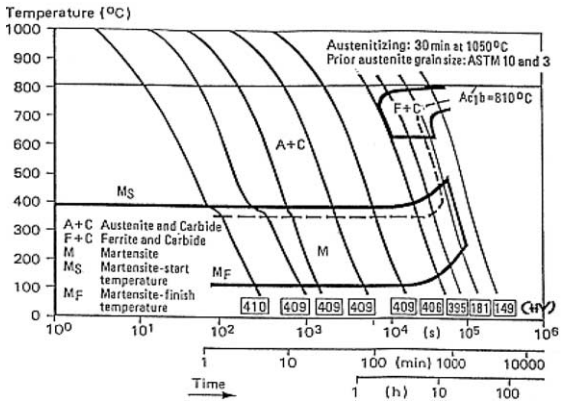

Fig. 1. Continuous cooling transformation diagram for steel G91 after [17].

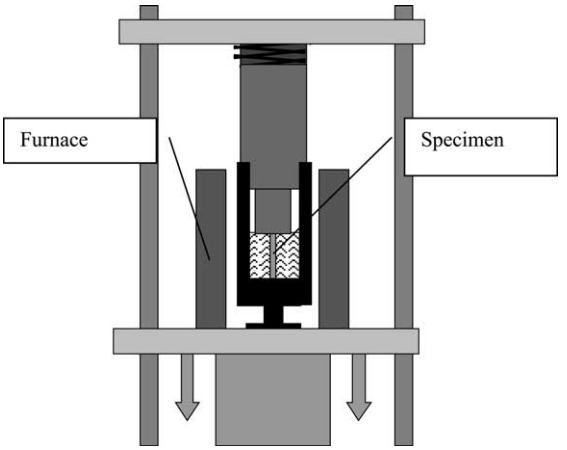

Fig. 2. Schematic view of the experimental set-up.

work and should not be reached for technological applications under standard working conditions. Once the specimen fractured, lead was removed from the fracture surfaces by dissolution in an appropriated solution of composition $1/3H_2O_2, 1/3CH_3CH_2OH, 1/3CH_3COOH$ in order to make fractographic observations.

The lead employed for tensile tests was 99.95% in purity.

2.3. Fractography and microstructure analysis

A 525 M Philips scanning electron microscope (SEM) in the secondary electron mode was used to undertake the fractographic analysis. When necessary, a Jeol 200 CX TEM was used for microstructural investigations, a Siemens Kristalloflex 810 diffractometer to record X-rays diffraction (XRD) patterns and an EDAX system linked to the SEM to perform chemical analysis of the observed surfaces.

3. Results

3.1. Specimen microstructure

Martensitic microstructure of the base material was evidenced by optical (Fig. 3) and TEM observations. It consists of laths that colonised the prior austenite grains during the air quench from 1323 K. The average prior austenite grain size is approximately 20 μm. The TEM examination of the laths structure displays a tempered martensitic microstructure containing dislocations arranged into cells. It is also seen that the lath boundaries are decorated with many precipitates. These are of the $M_{23}C_6$-type (with M = 64 wt% Cr, 4 wt% Mo, 32 wt% Fe), they are also present at the grain boundaries. They appear during the tempering [18]. Referring to the literature [18], two other types of precipitates are also contained in this microstructure: the MC-type distributed in the matrix (with M = 13 wt% V, 87 wt% Nb) that appears during the austenisation phase and the M_4C_3-type also distributed in the matrix (with M = 30 wt% Cr, 56 wt% V, 11 wt% Fe, 3 wt% Nb) that appears during the tempering phase.

The XRD study indicates a BCC crystallographic structure (with no measurable quadratic distortion) with a lattice parameter $a = 0.286$ nm.

The heat treatment HT1 where the temper temperature was 773 K changes the precipitation state and increases the steel hardness. Fig. 4 gives the evolution of the hardness as a function of the temper temperature for isochrone (1 h) treatments. A maximum of hardness of 400 HV30 was obtained for a temper temperature of 773 K. Such a sensitivity to the tempering is often reported in martensitic steels such as for 12% chromium martensitic steels [11]. According to these results, the temper

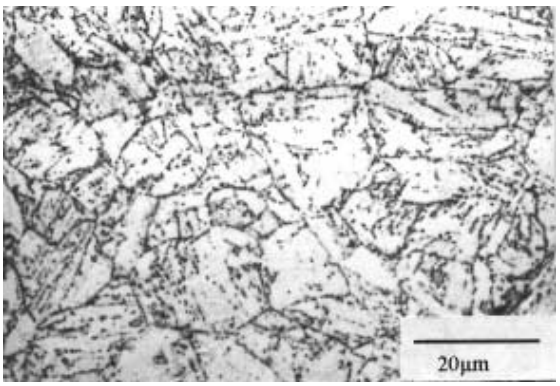

Fig. 3. Optical micrograph of the steel G91 in its standard state. The martensitic microstructure is recognised by the presence of laths in the prior austenitic grains of size about 20 μm.

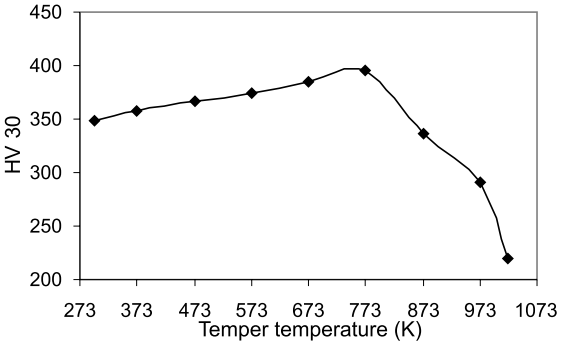

Fig. 4. Hardness evolution versus temper temperature of the steel G91 after a normalisation treatment at 1323 K for 1 h.

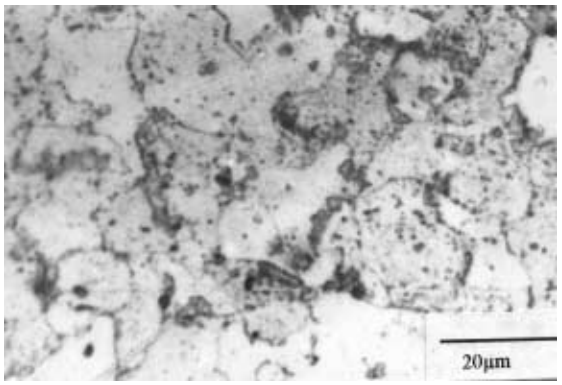

Fig. 5. Optical micrograph of the ferritic microstructure of Steel G91 after the heat treatment 2 with a grain size of about 20 μm.

temperature of the HT1-type specimens was chosen to obtain a high mechanical strength. Optical observations combined to XRD confirmed that HT1 did not induce any modification in prior austenite grain size and suggests that the transformation concerns only the nature and the distribution of the precipitates.

The second heat treatment HT2 is a cooling from the austenisation temperature to a temperature of 973 K which is maintained for 24 h. As predicted by the CCT diagram, the microstructure obtained is ferritic with many carbides at the grain boundaries (Fig. 5). The grain size remains approximately 20 μm and the hardness value is much smaller than for the martensitic microstructure, a result that is usually attributed to a lower dislocation density.

3.2. Tensile tests results

3.2.1. Heat treatment's influence and notch effect

Fig. 6 reports the engineering stress–strain curves obtained at 623 K for the different types of specimens.

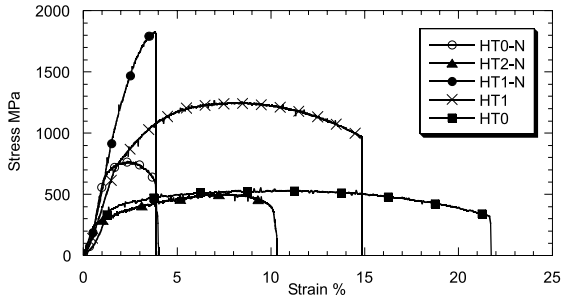

Fig. 6. Stress–strain curves for the different specimens in air environment at 623 K.

For the notched specimens the stress was defined as the ratio between the measured load and the notched section of 3 mm in diameter while for the smooth specimens, the stress was defined as the ratio between the recorded force and the transversal specimen section. The comparison between the behaviour of notched and smooth specimens must be done with care because the strain usually defined by the ratio between the specimen elongation and the initial length has a physical meaning as long as the deformation remains homogeneous, which is not the case in a notched specimen, at least in the plastic regime. A quick inspection of the curves reveals that:

(i) HT1 produces a reduction of plasticity and a quite high increase of strength. This is a consequence of the new precipitation state.

(ii) For notched specimens, the apparent elongation to fracture is considerably reduced. This is to a large extent due to the fact that the plasticity is localised around the notch area from the beginning of plastic deformation. Also, for a given heat treatment, the notched specimens exhibit higher levels of stress than the smooth ones. This is known as the notch effect and can be attributed to the stress triaxiality induced by the notch.

It is important to point out here that the level of tensile stress is highly increased by both HT1 and the notch effect. For the HT1-N specimen, the macroscopic yield stress increases from 300 to 1300 MPa.

The microstructural difference between ferritic and martensitic microstructure specimens is also clearly evidenced by their mechanical behaviour. It is clear from Fig. 6 that HT2-N is more ductile that HT0-N but has a reduced ultimate tensile strength. HT2 smooth specimen was not studied since we focused, for this particular microstructure, on specimens having the highest mechanical characteristics, i.e. the notched ones.

When tested in air, all the specimens exhibited a dimpled fracture surface characteristic of ductile fracture (similar to Fig. 8(a)). No striking differences are noticeable between the size or the depth of these dimples for all the types of specimens.

3.2.2. LME occurrence and the influence of the test temperature

The mechanical response of the HT0, HT0-N, HT1 and HT2-N specimens in liquid lead in the range of tested temperatures between 623 and 773 K did not differ from the in air one. Moreover the fracture surfaces remained always ductile. It can therefore be concluded that no LME occurs for these specimens in the given conditions. This is not the case for the HT1-N specimen. This clearly appears on the load–elongation (more realistic for notched specimen) curve of Fig. 7 as previously reported [9]. Failure occurs in liquid lead within macroscopic elastic behaviour without any evident macroscopic plasticity development. This change in the mechanical behaviour is also reflected in the fracture surfaces. Fig. 8(b) exhibits a 'flat' fracture surface in lead and from a macroscopic point of view, these specimens did not exhibit any necking indication. The fracture was transgranular with microfacets containing small rivers (Fig. 9) and corresponds to a cleavage-like transgranular failure. The fact that LME involves transgranular fracture was already published but it concerns cadmium polycrystals in liquid gallium [12], zirconium alloys in liquid mercury [13], polycrystalline pure magnesium in liquid-alkali metals [14], aluminium alloys in liquid mercury [15], K405 Ni-base superalloy in liquid bismuth–tin [16].

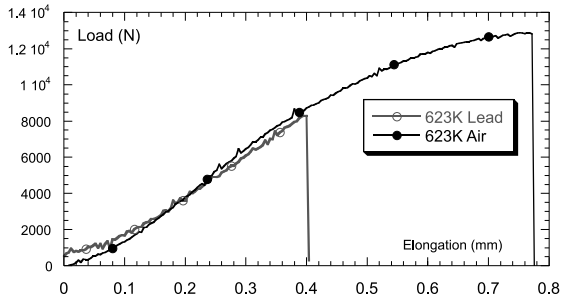

Fig. 7. Stress–strain curves on the HT1-N specimen in air and in liquid lead environment at 623 K.

Ductility is progressively recovered with the increasing of the test temperature as it can be seen in Fig. 10 where the area under the stress–strain curves is presented as an estimation of the mechanical work of fracture at different test temperatures for the HT1-N-type specimens, each point in the figure being an average of two measurements. It is clear that the HT1-N specimen undergoes an important embrittlement between 623 and 673 K whereas at 723 K the results obtained in air and in liquid lead almost coincide. This 'ductility trough' representation is quite common and was previously reported for other systems [2–5,19]. For temperatures

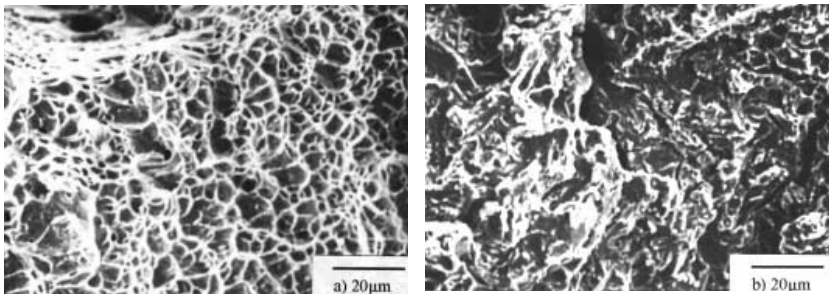

Fig. 8. SEM micrographs of the HT1-N specimen fracture surfaces for 623 K: (a) in air (ductile) with dimples; (b) in lead (brittle) flat with no dimples.

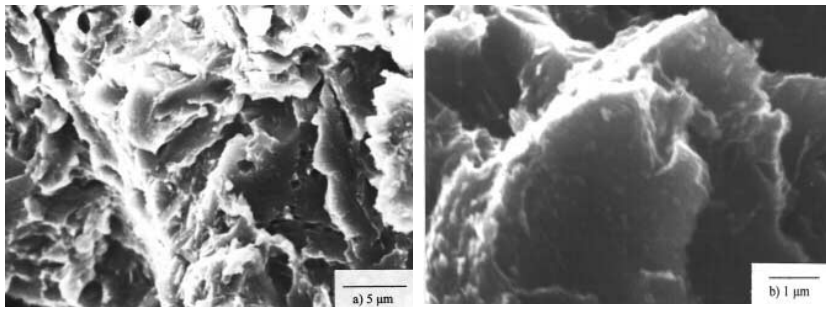

Fig. 9. SEM observations of the transgranular failure on some grains for HT1-N specimen at 623 K: (a) microfacets are evidenced; (b) higher magnification revealing the presence of small rivers.

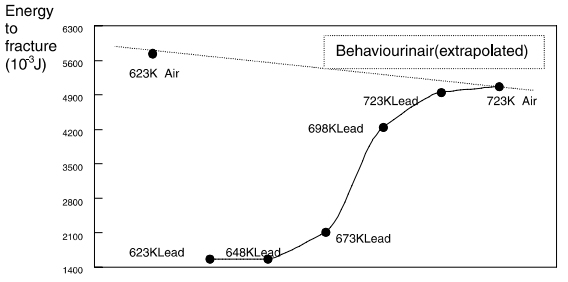

Fig. 10. Ductility trough for the HT1-N specimen in liquid lead between 623 and 698 K. Full ductility recovery for temperatures above 723 K.

above 623 K and below 723 K, the fractographic analysis shows a mixed brittle-ductile fracture surface as can be seen in Fig. 11. As the temperature increased, ductility recovered progressively from the middle of the specimens. At 723 K the fracture surface becomes fully ductile in agreement with the observed mechanical behaviour.

Finally, we would like to point out the existence of a layer of approximately 10 μm thickness between the liquid lead and the bulk steel for the HT1-N specimen as can be seen in Fig. 12. Note that the layer exhibits circumferential cracks, the influence of which will be discussed in the following section. Neither a careful EDAX analysis performed directly on this layer nor a structural analysis performed using XRD allows to conclude that this layer is an oxide. Rather, concerning this layer, the facts that:

(i) it has the same chemical composition as the base metal as revealed by the EDAX analysis;
(ii) it has the same crystallographic structure as the base metal as revealed by the XRD diffraction patterns;
(iii) the film is too thick to correspond to the natural chromium-oxide passive film;
(iv) the same type of layer can be observed by SEM on the HT1-N specimens tested in air, and also on HT0-N specimens, while it is absent on the HT1-type specimens (see Fig. 13);

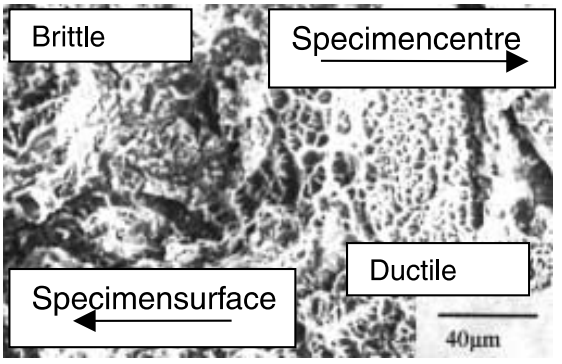

Fig. 11. SEM observation of a mixed fracture surface for HT1-N specimen at 673 K.

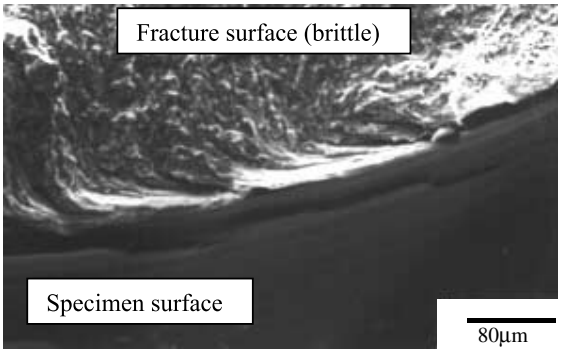

Fig. 12. SEM observation of the HT1-N specimen tested in liquid lead at 623 K. The cold-worked layer around the notch of the HT1-N specimen is clearly visible. Note many cracks on this layer.

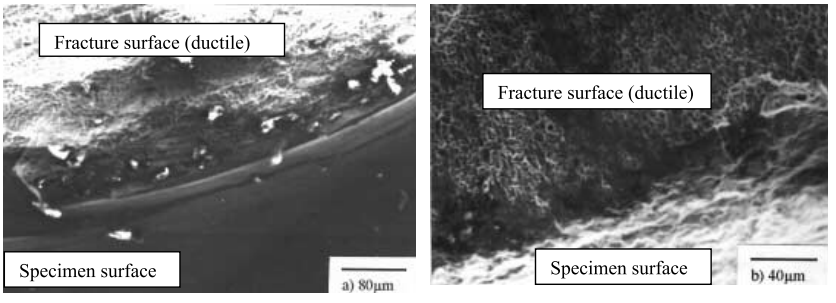

Fig. 13. (a) SEM observation on the HT0-N specimen tested in air at 623 K. The cold-worked layer around the notch of the HT1-N specimen is clearly visible. Note many cracks on this film. (b) SEM observation on the HT1 specimen tested in lead at 623 K. There is no apparent layer on this specimen surface.

(v) we cannot observe the film on specimens of the type HT2-N;

seem to indicate that the layers arise in specimens hard enough (HT0 and HT1 types) from the cold work induced by the mechanical machining of the notch. With these considerations, it can be deduced that the mechanically made layer should have two important properties as far as its mechanical properties are concerned:

(i) the film is harder and probably more brittle than the bulk whatever the heat treatment;

(ii) the film perfectly adheres to the bulk.

It is important to point out that we cannot exclude the presence of a natural chromium-oxide passive film predicted by the thermodynamics on our specimens' surfaces. Those films are known to be very thin (a few nm) and probably could not be detected using the experimental techniques employed in this work (EDAX, XRD and SEM observations) on the specimens tested from 623 to 723 K for the test times employed (less than 2 h). Concerning the eventual presence of lead-oxides for the specimens in contact with liquid lead, our experimental observations indicate that lead-oxide is present as ashes that usually float on the liquid lead bath surface.

4. Discussion

4.1. About the brittle failure

As it was previously exposed, the strategy adopted to perform this work was to investigate the influence of the hardness of the alloy (the other parameters as chemical composition of both liquid and solid metal for instance remaining constant) on the occurrence of LME. Two different situations need high load to deform a material. The first one results from a high yield stress, that is the resolved shear stress that produces dislocation motion. An increase of this shear stress naturally corresponds to an increase of the tensile stress producing it, and can be obtained for the material studied here by appropriate heat treatments. The second one is to introduce stress triaxiality. This ensures that the material yield shear stress will be reached for normal stresses higher than those triggering plasticity in the absence of stress triaxiality. A stress triaxiality can be produced by machining notches on cylindrical specimens. For applied stresses low enough, the stress triaxiality as well as stress concentration are located at the notch tip. When plastic deformation, that usually starts at the notch tip, reaches the centre of the specimens, then the stress triaxiality becomes maximum there according to Bridgman [17] and related models.

The brittle transgranular failure observed for HT1-N specimen suggests that failure may have propagated by cleavage. In this case, the important component of the stress tensor is the tensile stress normal to the fracture surface. Stoloff [12] has already discussed about how a liquid metal adsorption can reduce the interatomic bond strength at a crack tip and therefore leads to the propagation of a cleavage. Let us denote by σ_c the critical cleavage stress, that is the normal stress necessary to separate a given material in two parts. A well-known expression for σ_c is

$$\sigma_c = \sqrt{\frac{E\gamma_s}{a}},$$

where E is the Young's modulus, a the material lattice parameter assuming a cubic structure and γ_s the surface energy of the solid supposed isotropic. Taking typical values for the different parameters characteristic of the G91 steel ($E = 210$ GPa, $a = 0.286$ nm and $\gamma_s = 2.4$ J m^{-2} an average value for iron, the major chemical element of the steel) gives an estimate value for σ_c of about 40 GPa. As the surface energy of a solid comes from the lack of atoms at the surface, any adsorption thermodynamically favourable of new atoms may lead to a reduction of this energy. This is also known as the 'Rehbinder effect' [20]. Let us denote σ'_c the reduced cleavage stress corresponding to a reduced surface energy γ'_s. If cleavage is observed on a specimen tested in lead, this indicates that σ'_c is locally reached. To explain the fact that LME occurs only on the HT1-N specimens, the value of the normal stress σ_n at the notch tip that triggers the specimen failure at 623 K is evaluated. This value is obtained by multiplying the applied stress σ_a by the stress concentration induced by a notch K, given by the expression

$$K = 1 + 2\sqrt{\frac{d}{\rho}},$$

where ρ is the notch curvature radius and d the notch depth. Then $\sigma_n = K\sigma_a$ where σ_a is the applied stress we should have if the specimen were smooth (i.e. the ratio between the applied force and a smooth specimen surface). Taking into account the different correction terms, an estimate value for σ_n is 2800 MPa. Equating σ_n to σ'_c leads to a ratio γ'_s/γ_s near 0.5% a value too small to be realistic.

But let us observe the failure initiation site as shown in Fig. 12. The cold-worked layer exhibits many cracks whose tip is probably very sharp. Let us consider another damage process which starts first by the fracture of the layer being thus source of other stress concentration factors. This is suggested by the fact that this layer is probably very hard because of the high dislocation density introduced mainly by both the heat treatment and the notch machining. All these cracks may actually induce a higher stress concentration K' than K, the value

previously estimated. But in no case, this stress concentration alone cannot be held responsible for cleavage because they are also present on the HT1-N specimen, which is ductile, tested in air. The SEM pictures show that the layer has a thickness of about 10 μm. If we estimate the curvature radius of a microcrack in this layer to be about 0.1 μm, this leads to $K' \sim 21$, $\sigma'_c \sim 25000$ MPa and finally γ'_s/γ_s about 40%, a more sound value.

The layer may have played the same role on HT0-N specimen but in this case, the stresses seem to be relaxed by plastic deformation because the yield stress was not high enough. In order to assess the actual role played by the cold-worked layer, further mechanical tests including interrupted test are presently performed.

4.2. About the ductility recovery and the influence of the microstructure

The ductility recovery with increasing temperature can be simply explained by the well-known decrease of the yield stress with temperature. In our case this leads to the full disappearance of the embrittlement at 723 K. The experimental conditions (for which σ_y, the yield stress and σ'_c are close enough) may have led to the production of mixed fracture surfaces, dimpled in the middle of the specimens and brittle near the notch, that are effectively observed for temperatures ranging from 623 to 698 K. In this temperature range, ductility growth from the middle of the specimen and cleavage propagation from the surface, are competitive ways of stress relaxation. However this quick decrease of the σ_y over only 100 K could seem quite surprising. As we have seen before, the failure initiation stage of the bulk of the specimen is probably controlled by the mechanical behaviour of the cold-worked layer around it. When a microcrack from this layer reaches the bulk, it provides a sufficient local stress concentration to trigger the macroscopic fracture of the specimen. The temperature variation is also very influent on the mechanical parameters of the cold-worked layer and because this layer contains more entangled dislocations than the bulk, its $(\sigma_y)_{layer}$ is probably more sensitive to the temperature increase than the bulk. In this case, it is possible that, because the initiation stage is delayed, plasticity would have the possibility to develop and microvoids the possibility to grow from the middle of the specimen (where the triaxiality is the highest). Interrupted tests between 623 and 723 K and a detailed fracture analysis of the cold-worked layer that we are performing presently could confirm this hypothesis.

Considering now the role played by the microstructure, we have seen that under equivalent conditions of temperature and stress triaxiality, the specimens having a ferritic microstructure do not undergo any embrittlement by liquid lead. We believe that the main reason for that is that the HT2-N specimens have a much lower yield stress than the HT1-N ones and thus, that σ'_c cannot be reached for this type of specimen whatever the experimental conditions. Moreover no cold-worked layer was present on this specimen so that nothing could help an eventual brittle failure to initiate before the plastic development.

5. Conclusions

The main conclusions of this work can be summarised as follows:

1. A 9Cr 1Mo martensitic steel can be sensitive to liquid lead embrittlement.
2. The embrittlement of steel 91 occurs for a special combination of microstructural, geometric and loading conditions and does not depend on the contact time between the liquid metal and the solid one.
3. The transgranular failure observed suggests that LME of the steel 91 can be related to a lowering of the critical cleavage due to adsorption of lead.
4. In the case presented here, the cleavage nucleation may have been favoured by the presence of microcracks in the brittle layer produced by the mechanically machining of a notch on some of the specimens. This may have helped the local stress to reach σ'_c, the critical cleavage stress lowered by lead adsorption at these microcrack tips.

Acknowledgements

This work is a part of the material science research effort developed around spallation targets and hybrid nuclear reactor. It has been financially supported by the French CNRS GdR GEDEON and by EDF-Centre des Renardières-EMA department. We would like to thank D. Gorse from GdR GEDEON for valuable discussions and D. Vançon from EDF for his interest in our work. We are also indebted to P. Bocquet from Creusot-Loire-Industries for providing the steel used in our investigations.

References

[1] W.H. Johnson, Proc. Roy. Soc. Lond. 23 (1874–1875) 168, Republished in C.D. Beachem (Ed.), Hydrogen Damage, vol. 12, 1977, ASM.
[2] M.H. Kamdar, Progr. Mater. Sci. 15 (1973) 289.
[3] N.S. Stoloff, in: M.H. Kamdar (Ed.), Embrittlement by Liquid and Solid Metals, AIME, 1982.
[4] P.J.L. Fernandes, D.R.H. Jones, Int. Mater. Rev. 42 (6) (1997) 251.

[5] B. Joseph, M. Picat, F. Barbier, Eur. Phys. J. A.P. 5 (1999) 19.
[6] J.C. Lynn, W.R. Warke, P. Gordon, Mater. Sci. Eng. 18 (1975) 51.
[7] C.F. Old, P. Traverna, Metall. Sci. 13 (1979) 487.
[8] P.J.L. Fernandes, D.R.H. Jones, Eng. Failure Anal. 3 (1996) 299.
[9] A. Legris, G. Nicaise, J.B. Vogt, J. Foct, D. Gorse, D. Vançon, Scr. Mater. 43 (2000) 997.
[10] E.I. Rabkin, V.N. Semenov, L.S. Shvindlerman, B.B. Straumal, Acta Metall. Mater. 39 (1991) 627.
[11] G.R. Speich, AIME Trans. 245 (1969) 2553.
[12] N.S. Stoloff, T.L. Johnston, Acta Metall. 11 (1963) 251.
[13] B. Cox, Y.M. Wong, J. Nucl. Mater. 245 (1997) 34.
[14] S.P. Lynch, P. Trevena, Nat. Assoc. Corros. Eng. 44 (1998) 113.
[15] A.P. Reynolds, G.E. Stoner, Metall. Trans. 22A (1991) 1849.
[16] Z. Peidao, Y. Hai, Eng. Failure Anal. 3 (1996) 241.
[17] P.W. Bridgman, Trans. ASM 32 (1944) 533.
[18] C. Rasche, W. Bendick, J. Orr, ECSC Information Day (5.11.1992) Ed. British Steel Technical.
[19] W.R. Warke, K.L. Johnson, N.N. Breyer, Corrosion by Liquid Metal, Plenum, New York, 1970, p. 417.
[20] E.D. Shchukin, Colloids Surf. A 149 (1999) 529.